AFML-TR-72-47

MATERIALS PROCESSING OF RARE EARTH COBALT PERMANENT MAGNETS

P. J. JORGENSEN
R. W. BARTLETT
Stanford Research Institute

TECHNICAL REPORT AFML-TR-72-47

April 1972

AIR FORCE MATERIALS LABORATORY
AIR FORCE SYSTEMS COMMAND
WRIGHT-PATTERSON AIR FORCE BASE, OHIO 45433

DISCLAIMER NOTICE

THIS DOCUMENT IS BEST QUALITY PRACTICABLE. THE COPY FURNISHED TO DTIC CONTAINED A SIGNIFICANT NUMBER OF PAGES WHICH DO NOT REPRODUCE LEGIBLY.

NOTICE

When Government drawings, specifications, or other data are used for any purpose other than in connection with a definitely related Government procurement operation, the United States Government thereby incurs no responsibility nor any obligation whatsoever; and the fact that the government may have formulated, furnished, or in any way supplied the said drawings, specifications, or other data, is not to be regarded by implication or otherwise as in any manner licensing the holder or any other person or corporation, or conveying any rights or permission to manufacture, use, or sell any patented invention that may in any way be related thereto.

Copies of this report should not be returned unless return is required by security considerations, contractual obligations, or notice on a specific document.

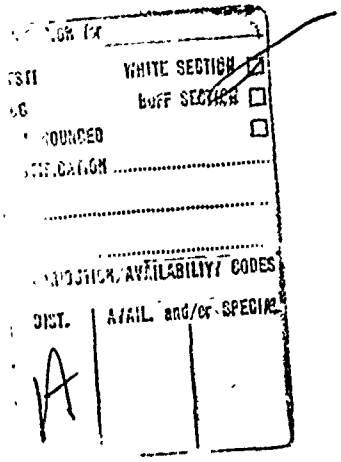

Unclassified

Security Classification

DOCUMENT CONTROL DATA - R & D

Security classification of title, body of abstract and indexing annotation must be entered when the overall report is classified

1 ORIGINATING ACTIVITY (Corporate author) Stanford Research Institute 333 Ravenswood Avenue Menlo Park, California 94025	2a. REPORT SECURITY CLASSIFICATION Unclassified 2b GROUP

3 REPORT TITLE

MATERIALS PROCESSING OF RARE EARTH-COBALT PERMANENT MAGNETS

4 DESCRIPTIVE NOTES (Type of report and inclusive dates)

Third Semi-Annual Interim Technical Report: July 1 to December 31, 1971

5 AUTHOR(S) (First name, middle initial, last name)

Paul J. Jorgensen
Robert W. Bartlett

6 REPORT DATE	7a. TOTAL NO OF PAGES	7b NO OF REFS
January 1972	56	9

8a CONTRACT OR GRANT NO	9a. ORIGINATOR'S REPORT NUMBER(S)
F33615-70-C-1624 b. PROJECT NO ARPA Order No. 1617 c. Program Code No. 0D10 d	PYU-8731 9b OTHER REPORT NO(S) (Any other numbers that may be assigned this report) AFML-TR-72-47

10 DISTRIBUTION STATEMENT

Approved for public release; distribution unlimited.

11 SUPPLEMENTARY NOTES	12 SPONSORING MILITARY ACTIVITY
	Air Force Materials Laboratory Wright Patterson Air Force Base Ohio 45433

13 ABSTRACT

Materials processing of rare earth-cobalt magnets ($RECo_5$) is being studied, including alternative methods of (1) alloy synthesis, (2) magnetic particle preparation, and (3) sintering. Evidence presented suggests that surface oxidation rather than mechanical stress is the cause of degradation in intrinsic coercivity. Apparatus using a zirconia electrochemical cell to determine the oxidation kinetics of rare earth cobalt alloys was constructed, and experiments were started on $SmCo_5$. Appreciable oxidation rates were measured at temperatures down to 105°C. Several plasma spheroidized and plasma annealed $RECo_5$ powder samples were sintered and magnetically evaluated. The results were compared with those from sintered specimens made from ball milled powders. $SmCo_5$ and $PrCo_5$ alloys were produced by metallothermic reduction. Coercivities of ball milled metallothermic powders were similar to those of the best arc melted and ball milled alloys. Sintering kinetic studies were made with $SmCo_5$ using a liquid phase sintering aid. Present results indicate that a phase boundary reaction leading to solution is the rate limiting step in sintering of $SmCo_5$.

DD FORM 1 NOV 65 1473 (PAGE 1)

S/N 0101-807-6801

Unclassified

Security Classification

14 KEY WORDS	LINK A		LINK B		LINK C	
	ROLE	WT	ROLE	WT	ROLE	WT
Magnetic Particles						
Rare Earth						
Cobalt						
Plasma Spheroidization						
Oxidation						
Sintering						

MATERIALS PROCESSING OF RARE EARTH COBALT PERMANENT MAGNETS

P. J. JORGENSEN
R. W. BARTLETT

ic

FOREWORD

This is the third semiannual interim technical report of the research program "Materials Processing of Rare Earth-Cobalt Permanent Magnets" under Contract F33615-70-C-1624. Stanford Research Institute project number is PYU-8731. This project is being conducted by the Materials Laboratory of Stanford Research Institute. Dr. Paul J. Jorgensen, Manager of the Ceramics Group, is the project supervisor. Dr. Robert W. Bartlett of Stanford University is project consultant. Dr. M. Nisenoff made the magnetic measurements. The research described in this report is part of the contractual research program of the Materials Physics Division, Air Force Materials Laboratory, Air Force Systems Command, Wright-Patterson AFB, Ohio. Mr. Harold J. Garrett (AFML/LPE) is the project monitor. It was sponsored by the Advanced Research Project Agency, ARPA Order No. 1617, Program Code No. 0D10.

This report covers research conducted between July 1 and December 31, 1971, and was submitted on March 6, 1972 by the authors for publication.

This technical report has been reviewed and is approved.

CHARLES E. EHRENFRIED
Major, USAF
Chief, Electromagnetic Materials Branch
Materials Physics Division
Air Force Materials Laboratory

ABSTRACT

Materials processing of rare earth-cobalt magnets ($RECo_5$) is being studied, including alternative methods of (1) alloy synthesis, (2) magnetic particle preparation, and (3) sintering. Evidence presented suggests that surface oxidation rather than mechanical stress is the cause of degradation in intrinsic coercivity. Apparatus using a zirconia electrochemical cell to determine the oxidation kinetics of rare earth cobalt alloys was constructed, and experiments were started on $SmCo_5$. Appreciable oxidation rates were measured at temperatures down to 105°C.

Several plasma spheroidized and plasma annealed $RECo_5$ powder samples were sintered and magnetically evaluated. The results were compared with those from sintered specimens made from ball milled powders. $SmCo_5$ and $PrCo_5$ alloys were produced by metallothermic reduction. Coercivities of ball milled metallothermic powders were similar to those of the best arc melted and ball milled alloys. Sintering kinetic studies were made with $SmCo_5$ using a liquid phase sintering aid. Present results indicate that a phase boundary reaction leading to solution is the rate limiting step in sintering of $SmCo_5$.

CONTENTS

ILLUSTRATIONS

TABLES

I INTRODUCTION

The objectives of this program are to investigate unconventional materials processing methods with the goal of achieving optimum properties of $SmCo_5$ and other $RECo_5$ compounds as permanent magnets. The primary problem is achieving high magnetic coercivity. Plasma spheroidization, and annealing of previously communuted particles, along with direct reduction from oxides and salts of the rare earths are being pursued to generate fine particles that can be magnetically aligned, compacted, and sintered by conventional techniques of powder metallurgy. The processing methods are being evaluated by determining the magnetic coercivity, chemical composition, homogeneity, particle size, and particle morphology of the resulting materials.

Studies to gain further knowledge of the liquid phase sintering process and magnetic evaluation of sintered alloys were begun during this research period. Because of the probable connection between oxidation and reduced magnetic coercivity a study of the oxidation kinetics of $SmCo_5$ was begun, emphasizing low oxygen pressures and both low and high temperatures. This is a continuing program and the results presented are essentially a progress report.

II DEGRADATION OF MAGNETIC COERCIVITY

Ball milling is capable of producing $SmCo_5$ with intrinsic coercivities in excess of 20,000 oersteds with good batch-to-batch reproducibility. Only one of ten ball mill runs on ten separate alloy melts yielded powder with an intrinsic coercivity below 20,000 oersteds, and that was 18,400 oersteds. The results of alloys processed and evaluated this period are summarized in Table I. It is apparent that comminuted powders and, therefore, mechanically stressed particles can have consistently high coercivities. Exposure in air for six days at room temperature does not degrade the coercivity (see arc melt No. 37 listed in Table I). However, high temperature annealing in air or under attainable vacuum is deleterious. The only exception observed in our laboratory, or reported by other investigators, occurred when the $SmCo_5$ particle was wetted by a liquid film of either calcium or an alloy containing more samarium than the magnetic particle.

Only calcium and thorium have a lower oxide free energy of formation, and both calcium and a richer samarium alloy have a slightly lower equilibrium oxygen pressure than $SmCo_5$ and would be able to remove oxygen from $SmCo_5$ at temperatures above their liquidus. The equilibrium oxygen pressures are several orders of magnitude below those attainable under the best vacuum conditions, and residual oxygen in an evacuated enclosure will react with $SmCo_5$ unless the samarium or calcium protective liquid film completely envelops the particle. When there is a space between the samarium or calcium getter and $SmCo_5$, oxygen transfer cannot occur because the equilibrium oxygen partial pressure is too low for an adequate gas phase mass transfer rate. This was experimentally verified when $SmCo_5$ powder with a measured intrinsic coercivity of 21,800 oersteds was heated

Table I

MAGNETIC PROPERTIES OF COMMINUTED POWDERS*

Alloy	Arc Melt No.	Ball Mill Grinding (hr)	H_M(kOe)	H_C^M (kOe)	$4\pi M_r$ (Gauss)	Remarks†
$SmCo_5$	33	3	54	21.8	6,950	
$SmCo_5$	33	3	50	1.5	4,500	Powder heated under vacuum with calcium chips 2-1/2 hr at 700°C
$SmCo_5$	35	3	55	23.4	7,660	
$SmCo_5$	36	3	56	18.4	8,500	
$SmCo_5$	37	10	61	26.1	7,000	
$SmCo_5$	37	10	64	26.5	9,640	Powder exposed in air 6 days at 25°C
$SmCo_5$	Commercial Alloy	Commercial TWT Manufacturer	60	7.14	8,760	
$PrCo_5$	39	3	61	3.86	12,800(?)	
$PrCo_5$	39	10	60	2.86	6,530	Apparently overground

* Magnetic results were determined in a uniform procedure for all materials by setting in epoxy under a 27,000 oersted aligning field.

† Except where noted the powders were epoxy bonded within 48 hours after comminution.

inside vacuum to 700°C in the presence of calcium chips. The intrinsic coercivity decreased to 1500 oersteds (see Table I). It is apparent that either the thermal treatment itself or very small amounts of residual gashave a drastic effect on the nucleation of new domains or on domain wall migration that determine coercivity.

Since intrinsic coercivities actually can be improved significantly by heating a $SmCo_5$ particle surrounded by a calcium or samarium rich film, as is done in all of the successful sintering methods, it is concluded that thermal effects alone are not causing the degradation. It is also clear from the reduced coercivities resulting from plasma annealing, in which the particle is heated for a few seconds at most and is not melted, that substantial diffusion of deleterious gases inward from the particle surface is not necessary to cause the reduction in coercivity. Hence, an extremely small amount of gas, probably oxygen, reacting at the surface appears to have a marked effect in initiating the nucleation of new magnetic domains at the particle surface. A similar hypothesis has been proposed by Becker.[1]

The effect of particle size on the intrinsic coercivity of ball milled $SmCo_5$ and $PrCo_5$ powders was studied, and the results are summarized in Table I. Ball milling of $SmCo_5$ for three hours after crushing to pass a 30-mesh screen yields particles having an average particle size of 4 to 5 microns and an average intrinsic coercive force of 22,000 oersteds. Increasing the milling time to 10 hours decreases the particle size to 2 to 3 microns and raises the intrinsic coercivity to 26,000 oersteds. The average sizes were determined using a Fisher subsieve analyzer.

Ball milled $PrCo_5$ shows a lower intrinsic coercivity when milled 10 hours (2 to 3 microns) than when milled only three hours (about 5 microns). This overgrinding effect for $PrCo_5$ is substantially in agreement with the results using attritor milling that have been reported by

Strnat and coworkers[2] and Becker.[3] However, the reduction in coercivity may be caused by further surface reaction as grinding proceeds rather than mechanical stress as has been previously assumed.

A commercial $SmCo_5$ alloy powder produced by melting and comminution was also evaluated, and the results are reported in Table I. This magnet powder has an intrinsic coercivity of only 7140 oersteds. However, it should be noted that this material is currently being used to produce $SmCo_5$ magnets for traveling wave tubes with much higher final coercivities than the starting powder. Again, these higher coercivities result from liquid phase sintering with a samarium rich alloy that also getters oxygen.

The intrinsic coercivities obtained with comminuted powders may depend on the care taken to eliminate oxygen during grinding. Sodium-gettered hexane is being used as the milling fluid in our laboratory. The ball mills are loaded and sealed while in an argon glove box so that the hexane and rare earth alloy are not exposed to oxygen during grinding. Recent oxidation studies with $SmCo_5$, which will be discussed in a later section, show that the alloy is very reactive with oxygen even at temperatures near room temperature.

III PLASMA TREATED $RECo_5$ POWDERS

An extensive program of processing samarium and praseodymium alloys of cobalt by heating dispersed alloy particles in an inert gas plasma has been underway. Both annealing below the particle melting point and melting and quenching (spheroidization) have been employed. The apparatus and experimental processing method have been previously described.[4]

A. Evaluation of Particles

The plasma spheroidization process requires large amounts of argon, and because intrinsic coercivities appeared to be extremely sensitive to small amounts of surface oxidation, the plasma apparatus was equipped with a solid state zirconia electrochemical cell to continuously monitor the oxygen partial pressure in the process gas. The bottled argon had an oxygen partial pressure of about 3.5×10^{-5} atm. In early experiments this gas flowed through a heated bed of calcium chips (4 in. dia. x 20 in. high). Monitoring with the zirconia oxygen gage indicated that the oxygen partial pressure was lowered at modest argon flow rates but at the normal operating flow rates the oxygen level was not appreciably lowered by the calcium chips. However, operation of the plasma system with injection and spheroidization of $SmCo_5$ particles was lowering the effluent oxygen pressure to approximately 10^{-22} atm. At normal particle and gas feed rates, this corresponds to an oxygen accumulation by the spheroidized particles of about 0.1 wt%.

Two calcium chip getter furnaces were installed in the plasma spheroidization feed gas line to decrease the oxygen partial pressure of the argon plasma. Oxygen partial pressures in the process feed gas are now maintained below 10^{-16} atm, and the oxygen partial pressure is

constantly monitored during each plasma spheroidization or plasma annealing experiment with the zirconia electrochemical cell. The effluent gas is monitored before, during, and after injection of the particles.

Bulk oxidation of the $SmCo_5$ during processing is insignificant. Surface oxidation cannot be calculated for the plasma spheroidized material because a considerable fraction of the total surface area is contributed by the submicron particles of the fume. During plasma annealing, no fume is formed and, for a 4-micron particle, the oxygen surface concentration can be no greater than about 2 molecular layers of O_2 at an oxygen pressure of 10^{-16} atm. This calculation assumes that all of the residual oxygen is gettered by the particles.

Magnetic properties of plasma spheroidized and plasma annealed $SmCo_5$ and $PrCo_5$ samples are shown in Table II. Both plasma annealing and spheroidization substantially lower the intrinsic coercivities of $SmCo_5$. Spheroidization (melting) lowers the coercivity slightly more than does plasma annealing. The remanent magnetization of the spherical particles is reduced because some are not single crystals, and, therefore, perfect alignment cannot be achieved. The data from Table II were compared with previous magnetic results on plasma annealed and plasma spheroidized $SmCo_5$ conducted at higher residual oxygen pressures.

The lowered oxygen pressure of the recent experiments had statistically no effect on the intrinsic coercivities that were achieved. It is clear from these results that if the surface oxidation hypothesis of the preceding section is valid, extremely small amounts of oxygen are sufficient to cause severe reduction of the intrinsic coercivity. Both plasma annealing and spheroidization also lowered the intrinsic coercivities measured with $PrCo_5$.

Table II

MAGNETIC PROPERTIES OF PLASMA SPHEROIDIZED AND PLASMA ANNEALED POWDER

Run No.	Alloy (Nominal)	Initial Composition	Arc Melt No.	Ball Mill Grinding (hr)	Plasma Oxygen Pressure (atm)	Anneal/ Spheroidize	H_M (kOe)	$_MH_C$ (kOe)	$4\pi M_r$ (Gauss)	Remarks
P-33	$SmCo_5$	36% Sm	33	3	--	Spheroidized	51	3.64	3101	
P-33	$SmCo_5$	36	33	3	--	Spheroidized	47	3.85	2540	Powder exposed to air two weeks at room temperature
P-38	$SmCo_5$	36	36	10*	$1x10^{-5}$†	Spheroidized	58	7.14	6600	
P-46	$SmCo_5$	36	37	10	$2x10^{-16}$	Spheroidized	60	8.13	4020	
P-47	$SmCo_5$	36	37	10	$2x10^{-16}$	Spheroidized	58	3.6	3530	Rerun of previous spheroidal material
P-48	$SmCo_5$	36	45	3	$2x10^{-16}$	Spheroidized				
P-39	$SmCo_5$	36	36	10	$2x10^{-16}$	Annealed	58	8.7	8050	
P-37	$SmCo_5$	36	36	10	--	Annealed	58	11.3	8280	
P-44	$SmCo_5$	36	37	10	$3x10^{-19}$	Annealed	61	11.4	6710	
P-42	$PrCo_5$	33	39	10	$3x10^{-19}$	Spheroidized	59	1.43	3900	
P-43	$PrCo_5$	33	39	10	$3x10^{-19}$	Annealed	58	1.71	5050	
P-34	$PrCo_5$	33	39	10	--	Annealed	48	1.64	3490	

*Ball milled with iron balls.

†Prior to installation of additional calcium getter furnace.

The magnetic evaluation of loose powders requires curing an epoxy binder while in a particle aligning magnetic field. Tests were made using a uniform sample of plasma annealed $SmCo_5$ to determine if variations in the curing procedures were affecting the measured coercivity. Curing time and alignment field were varied but these parameters did not have an effect on the measured coercivity. The results are summarized in Table III.

B. Evaluation of Sintered Magnets Made From Plasma Treated Powders

The final evaluation of plasma spheroidization and plasma annealing must be accomplished by fabricating the treated powders into magnets and measuring the magnetic properties of the sintered compacts.

The powders were blended with a 60% Sm-40% Co sintering additive and aligned in a magnetic field of 24 kOe. The samples were contained in rubber bags inside of perforated nonmagnetic tubes and following alignment were isostatically pressed at 50,000 psi. Samples were also formed by uniaxial die pressing in a magnetic field of 50 to 10 kOe.

The sintering was done in a graphite heated vacuum furnace that had been repeatedly filled with gettered argon and evacuated. The atmosphere during sintering was oxygen-gettered argon, and the sintering temperature was 1130°C. A postsintering aging treatment at 900°C for 4 hours was used to increase the intrinsic coercive force.

The results of sintering the plasma spheroidized and plasma annealed materials following die pressing in a magnetic field are shown in Table IV. The magnetizing field for all of the samples was 60 kOe.

Initial plasma spheroidization experiments resulted in spherical material that contained $SmCo_5$ and Sm_2Co_{17} phases, as a result of the losses in samarium during spheroidization. The amount of Sm_2Co_{17} was small, and the magnetic remanence was reduced. Sintering these early materials with

Table III

EFFECT OF EPOXY CURING CONDITIONS ON MAGNETIC PROPERTIES OF PLASMA ANNEALED $SmCo_5$ POWDER

Powder*	Curing Time	Curing Temperature (°C)	Curing Alignment Field (kOe)	H_M (kOe)	$_MH_C$ (kOe)	$4\pi M_r$ (Gauss)
P-Run 36	4	40	27	56	11.1	7270
P-Run 36	4	40	0	58	14.1	4120
P-Run 36	9	40	27	58	14.0	7580
P-Run 36	20	40	27	56	11.1	6400
P-Run 36	20	40	0	58	14.1	4120

*The plasma starting powder was taken from arc melt No. 35 ball milled three hours.

Table IV

MAGNETIC PROPERTIES OF SINTERED MAGNETS
FABRICATED FROM PLASMA SPHEROIDIZED
AND PLASMA ANNEALED MATERIALS

Sample No.	Powder No. (see Table II)	Composition*	Particle Processing (Anneal/Spheroidize)	$_{M}H_{C}$ (kOe)	$4\pi M_r$† (Gauss)	Alignment‡ Factor
SL-27	p38	$SmCo_5$	Spheroidized	3.14	3020	-
SL-39	p38	$SmCo_5$	Spheroidized	2.5	3360	0.47
SL-32	p46	$SmCo_5$	Spheroidized	9.1	2720	-
SL-45	p46	$SmCo_5$	Spheroidized	15.0	3100	0.65
SL-33	p47	$SmCo_5$	Spheroidized	3.64	2360	-
SL-5	p48	$SmCo_5$	Spheroidized	25.7	4650	0.94
SL-28	p39	$SmCo_5$	Annealed	3.1	5380	0.80
SL-38	p39	$SmCo_5$	Annealed	4.14	5000	0.73
SL-26	p37	$SmCo_5$	Annealed	7.28	3610	-
SL-41	p37	$SmCo_5$	Annealed	5.6	4990	0.75
SL-31	p44	$SmCo_5$	Annealed	7.4	4500	-
SL-37	p44	$SmCo_5$	Annealed	8.15	4820	0.71
SL-29	p42	$PrCo_5$	Spheroidized	-	0	-
SL-43	p43	$PrCo_5$	Annealed	-	0	-
SL-34	p34	$PrCo_5$	Annealed	17.1	4230	0.70
SL-40	p34	$PrCo_5$	Annealed	19.7	7720	0.90

*All magnets were formed with 20 percent of sintering aid (60% Sm - 40% Co)

†The alignment factor was obtained by dividing $4\pi M_r$ by $4\pi M$ at 60 kOe

‡No adjustment was made for the volume occupied by the sintering aid, and these values have not been corrected for demagnetization effects.

an enriched samarium-cobalt alloy as a sintering aid did not result in magnets with properties comparable to magnets formed from powders produced by comminuting arc melted ingots.

Adjustment of the plasma temperature and duration of heating in the plasma resulted in minimal samarium losses during plasma spheroidization, and spherical single phase, $SmCo_5$, particles were achieved. The magnetic remanence of these materials (see sample SL-5, Table IV) was low, as a result of the polycrystalline nature of the spherical particles. On cooling from the liquid phase, several grains are nucleated within each droplet, and since these grains are randomly oriented, it is impossible to achieve good magnetic alignment and this results in low remanence. Experiments to achieve improved alignment by heat treating at 820°C for 75 hours to allow grain growth to occur to produce fewer grains in the spherical particles that can be magnetically aligned have not been successful. A careful examination of sectioned $SmCo_5$ plasma produced spheres and microstructures of magnets produced from these plasma spheroidized materials show some single crystalline spheres and many polycrystalline spheres. The polycrystalline spheres following grain growth heat treatments contain equiaxed grains usually numbering between four and eight grains per sphere.

Annealing of $PrCo_5$ in a plasma did not produce high coercive force powder material immediately following plasma annealing. However, when these powders were sintered at 1130°C, using a samarium cobalt sintering aid, the intrinsic coercive force of the resulting magnet was 19,700 oersteds (see Table IV, sample No. SL-40). The $4\pi M_r$ value was only 7720 Gauss indicating incomplete alignment. This material was composed primarily of single crystal particles.

By sintering ball milled arc melted $SmCo_5$ and $SmCo_5$ material both produced in our laboratory and supplied by a manufacturer of traveling wave tube magnets, we were able to compare the magnetic properties of

sintered compacts obtained using ball milled powders and with plasma treated powders. The results for ball milled powders after sintering are presented in the next section.

IV SINTERED MAGNETS FROM BALL MILLED POWDERS

The magnetic results obtained with sintered magnets made from ball milled powders are shown in Table V. With comminuted material, the best coercivities are obtained with relatively coarse powder. Specimen SL-4 with the highest values of coercivity was milled only 2 hours. This sample was made by adding the sintering aid as a fine powder, which had been previously ball milled 6 hours, to -30 mesh $SmCo_5$ and then grinding the mixture for 2 additional hours. The sintering aid was a 60% Sm-40% Co alloy. The oxygen content in this sintered sample (SL-4) was 1.17%, determined by neutron activation analysis, but much of this is presumed to be in the nonmagnetic matrix. Evidence that the alignment is unsatisfactory can be seen in Figure 1, which is a magnetization loop for sample SL-4. The $4\pi M$ values started falling immediately on entering the second quadrant, and the loop was asymmetric and unsaturated. The starting material had an intrinsic coercive force of greater than 20 kOe, and this high coercivity may be part of the alignment problem. Work during the next period will include alignment studies and methods for easily achieving satisfactory alignment.

It is clear that for $SmCo_5$ at least, high coercivities can be obtained in sintered magnets using ball milling for particle preparation.

Table V

MAGNETIC PROPERTIES OF ISOSTATICALLY PRESSED AND VACUUM SINTERED SAMARIUM-COBALT MAGNETS* MADE FROM BALL MILLED POWDERS

Sample No.	$SmCo_5$ Preparation	Sintering Aid	Max. Sintering Temp. (°C)	H_M (kOe)	H_{MC} (kOe)	$4\pi M_r$ ‡ (Gauss)
SL-2	Ball milled 1 hr	60% Sm alloy†	1130	57	17.2	5260
SL-4	Ball milled 2 hr	60% Sm alloy	1130	67**	32.8	6020
SL-3	Ball milled $3\frac{1}{2}$ hr	60% Sm alloy	1130	57	5.7	5820
	Commercial TWT Manufacturer (ball milled)	Commercial TWT Manufacturer	1100	57	28.3	4850

*The magnets were aligned in a 24,000 oersteds field, isostatically pressed at 50,000 psi, sintered 5 minutes at the maximum temperature, and aged 3 hours at 900°C.

†The sintering aid was about 12 wt% of the material and was previously ball milled 6 hours.

‡No adjustment was made for the volume occupied by the sintering aid

**Saturation was not achieved at the maximum field strength available.

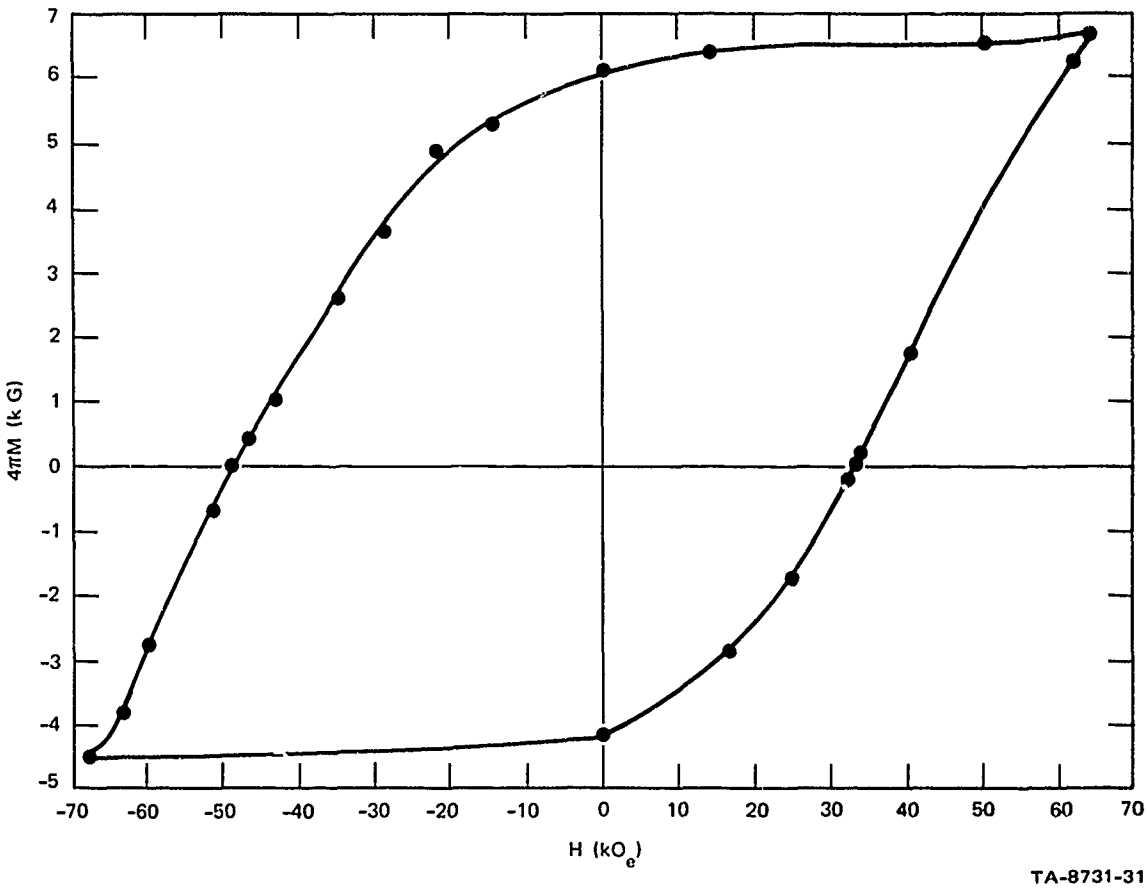

FIGURE 1 MAGNETIZATION CURVE FOR SINTERED $SmCo_5$: SPECIMEN SL-4

V ALTERNATIVE POWDER PREPARATION METHODS

Because the strain-induced defect model of nucleation and migration of domains in rare earth-cobalt magnetic alloys appears to be less viable than earlier investigations indicated, there is less incentive to pursue processing methods that produce strain-free particles or to pursue comminuted particle annealing studies.

Work is continuing on direct reduction of rare earth salts metallothermically to produce an alloy sponge with suitable magnetic properties. This is a potentially less expensive method for producing $RECo_5$ alloys than the conven ional sequence of rare earth metal purification followed by vacuum arc melting of the alloy.

A preliminary thermochemical study was made of potential processes for metallothermic reduction of oxides and halides of cobalt and samarium to form the $SmCo_5$ alloy. The other rare earths will have similar thermodynamic behavior. Particular attention was paid to systems in which the metallothermic reaction product is a two-phase mixture of $SmCo_5$ particles and a salt or slag phase that can subsequently be leached, or otherwise chemically processed, to extract the salt or slag without adversely affecting the $SmCo_5$ particles.

Free energy data for the formation of oxides, fluorides, and chlorides are presented in Tables VI through VIII, respectively. The data are usually for 1227°C, and they are arranged in order of ascending free energy of formation. Hence, any metal in a series should reduce the salts of the metals below it in that series at the temperature indicated. For each table, the most stable compounds have been selected.

Only calcium and thorium are possible reductants for the rare earth oxides and the latter is slightly radioactive. Calcium, barium, and

Table VI

GIBBS FREE ENERGY FORMATION OF
SELECTED OXIDES AT 1500K

Oxide	$\Delta G \left(\frac{cal}{mole}\right)$	$\Delta(\Delta G)$	
CaO	-115,500	0	$BP_{Ca} = 1480^{o}C$
Ba_2O	-113,000	2,500	$BP_{Ba_2O} = 800^{o}C$
$\frac{1}{2}ThO_2$	-112,500	3,000	
$1/3La_2O_3$	-112,500	3,000	
$1/3Sm_2O_3$	-112,000	3,500	
$1/3Pr_2O_3$	-111,500	4,000	
$1/3Ce_2O_3$	-105,500	10,000	
$1/3Y_2O_3$	-103,700	11,800	
MgO	-102,000	13,500	
$\frac{1}{2}ZrO_2$	-97,500	18,000	
Li_2O	-96,500	18,500	

Table VII

GIBBS FREE ENERGY OF SELECTED FLUORIDES AT 1500K

Fluoride	$\Delta G \left(\frac{cal}{mole}\right)$	$\Delta(\Delta G)$
$\frac{1}{2}CaF_2$	-115,500	0
$\frac{1}{2}BaF_2$	-115,000	500
LiF	-115,000	500
$1/3PrF_3$	-110,000	5,500
$1/3SmF_3$	-105,000	10,500

Table VIII

GIBBS FREE ENERGY OF SELECTED CHLORIDES AT 1500K

Chloride	$\Delta G \left(\frac{cal}{mole}\right)$	$\Delta(\Delta G)$
LiCl	-76,000	0
$\frac{1}{2}BaCl_2$	-74,000	2,000
$\frac{1}{2}SmCl_2$	-72,000	4,000
$\frac{1}{2}CaCl_2$	-72,000	4,000
$1/3SmCl_3$	-62,000	14,000

lithium are suitable reductants for the rare earth fluorides. Rare earth chlorides cannot be reduced by any metal with the exception of lithium and barium, but the free energy margin, $\Delta(\Delta G)$, is slight. The bromides and iodides do not appear to provide any system for metallothermic reduction of the corresponding rare earth salts.

Metallothermic reduction requires an intimate stoichiometric mixture of fine powders of (1) the rare earth salt, (2) cobalt or a cobalt salt, and (3) the reducing metal. The salts are brittle solids that can be readily ground. Cobalt can be obtained in powder form. Malleable metal reductants can be converted to brittle hydrides and then ground to yield fine powders. The alkali and alkaline earth hydrides generally decompose on heating before or simultaneously with the reduction reaction.

In preliminary experiments, samarium-cobalt alloy particles have been produced by reduction in a $SmF_2/LiF/BaF_2$ salt phase but difficulties were encountered in dissolving the salt without damaging the alloy particles dispersed in it.

The alloys $SmCo_5$, $PrCo_5$, $Sm_{0.5}Pr_{0.5}Co_5$, $Sm_{0.5}MM_{0.5}Co_5$, $Sm_{0.5}Y_{0.5}Co_5$, and $Sm_{0.5}La_{0.5}Co_5$ were produced by calcium reduction of a stoichiometric mixture of hydrided calcium, rare earth oxides, and cobalt powders. The metallothermic reduction reaction was conducted in an iron retort heated in argon at various temperatures, depending on the composition, for two hours. After dilute hydrochloric acid leaching of the charge to remove CaO, a $RECo_5$ sponge with a particle size of about 35 mesh remained.

The x-ray diffraction pattern of the $SmCo_5$ sponge exhibited little line broadening and indicated that the alloy was more homogeneous and less strained than alloys produced by arc melting and quenching. With the exception of a trace of Sm_2Co_7, there was no other phase detected. However, some of the mixed alloys indicate that considerable RE_2Co_{17} is present.

Sieving the $SmCo_5$ sponge before any grinding yielded a trace of -20μm particles, but these were not magnetic and are probably unleached CaO. A neutron activation analysis shows the oxygen content to be 0.170% after grinding, which is similar to arc melted $SmCo_5$. Part of the oxygen assay is probably the result of residual CaO.

Ball milled $SmCo_5$ sponge has magnetic properties similar to arc melted $SmCo_5$ after milling. The intrinsic coercivity was 21,400 oersteds. The remanence of sintered magnets of $SmCo_5$ was reduced because of inadequate liberation of fine single crystals during ball milling (two hours) that prevented ideal magnetic alignment. Polycrystalline $SmCo_5$ grains are shown among the ground particles in Figure 2.

Metallothermically reduced $PrCo_5$ and mixed rare earth cobalt alloys containing samarium will be ball milled and evaluated magnetically. We are particularly interested in the effect of composition and processing on intrinsic coercivities. If satisfactory coercivities can be obtained, attempts will be made to prevent the production of subcritical-sized crystals during the thermite reduction step and subsequent heat treatments.

FIGURE 2 BALL MILLED $SmCo_5$ ALLOY PARTICLES REDUCED BY CALCIUM

VI SINTERING SHRINKAGE KINETICS

A. Introduction

A sintering study of samarium-cobalt powders was undertaken to determine the parameters that control the sintering process. The sintering procedures currently used entail addition of a samarium rich phase (60% Sm-40% Co). This additive becomes liquid during the sintering process, and therefore liquid phase sintering kinetics are to be expected. A liquid phase to promote sintering in metallic systems has been used for many years,[5] and a review of this area was provided by Lenel[6] in 1948. The liquid phase sintering process may be divided into three stages: (1) rearrangement on formation of the liquid phase, (2) solution and precipitation of the solid phase, and (3) coalescence or solid phase sintering with the formation of a solid skeleton.

When the liquid phase first becomes molten it tends to coat the solid particles. If complete wetting occurs, the solid-vapor interface is eliminated. Therefore, the driving force for densification is the reduction of the liquid-vapor surface area and consequently a decrease in the total surface energy. Kingery[7] has derived equations to describe liquid phase sintering during the solution-precipitation stage, assuming spherical particles, complete wetting of the solid by the liquid, solution of the solid in the liquid phase, and constant grain size. The rate controlling step could be diffusion in the liquid phase or the phase boundary reaction leading to solution.

The equation that describes diffusion controlled sintering is

$$\Delta L/L_o = \left(\frac{6k_2 \, \delta \, DC_o \, \gamma_{lv} \, V_o}{k_1 \, RT} \right)^{1/3} r^{-4/3} t^{1/3} \qquad (1)$$

where k_1 and k_2 are constants approximately equal to 1/2 and 1, respectively; δ is the thickness of liquid film between particle-particle contact points; D is the diffusion coefficient of the slowest diffusing solute species in the liquid phase; C_o is the solubility at infinite radius of curvature; γ_{lv} is the liquid vapor surface energy; V_o is the molecular volume; r is the particle radius; t is time; and $\Delta L/L_o$ is the linear shrinkage.

A similar expression describes liquid phase sintering when the process is controlled by the phase boundary reaction, i.e.,

$$\Delta L/L_o = \left(\frac{2k'k_2 \gamma_{lv} C_o V_o}{k_1 RT} \right)^{\frac{1}{2}} r^{-1} t^{\frac{1}{2}} \qquad (2)$$

where k' is the appropriate reaction rate constant. Reaction rates can be predicated for diffusion controlled sintering, but because of our lack of knowledge of the reaction rate constant, k', in equation (2), it is impossible to predict a quantitative rate if the process is controlled by the rate of dissolution.

Measurement of linear shrinkage as functions of time, temperature, and particle size provides a means to distinguish between the two rate controlling processes. The linear shrinkage of $SmCo_5$ containing 20% additive (60% Sm-40% Co) has therefore been measured as a function of time.

B. Experimental Procedure and Results

Cylindrically shaped specimens, 0.32 cm in diameter by 1.0 cm long, were fabricated by die pressing at 30,000 psi in a magnetic field of 5,000 to 10,000 oersteds. The specimens were placed on a molybdenum support in a furnace employing a graphite heater surrounded by oxygen gettered argon. The shrinkage was recorded by time lapse photography,

and the data were taken from the films by means of a Telereadex film analyzer.

Since the solution-precipitation stage in which we are interested is preceded by a rearrangement stage, selection of the value for L_o becomes extremely important. Prill et al.[8] have shown that errors of interpretation can occur if L_o is not properly determined. That is, the exponent on time is reduced when the shrinkage occurring during the rearrangement process is not considered. In our studies, we found that a heat-up time of approximately 2 minutes to temperatures near 1100°C was sufficient to include the major portion of the rearrangement process; L_o was then taken and the corresponding time was defined as time zero. A plot of the data obtained at 1125°C is shown in Figure 3, and these data are typical of data obtained between 1100 and 1200°C.

A superior fit to the initial data, the data supposedly corresponding to the solution-precipitation stage, is obtained with a line having a slope of 1/2 instead of 1/3. Slopes of 1/2 always fit the data better than slopes of 1/3.

C. Discussion

Equation (2) appears to fit the shrinkage versus time data better than equation (1), suggesting that the sintering of $SmCo_5$ is controlled by the phase boundary reaction leading to solution and not by diffusion in the liquid phase. Increasing the temperature from 1125°C to 1155°C did not result in a perceptible increase in the rate of sintering, i.e., the intercept values on a logarithm shrinkage versus logarithm time plot remained unchanged. This behavior is not surprising if we consider possible values for the energy of activation of the temperature and the small temperature difference.

The shrinkage corresponding to the plateau in Figure 3 is 4%.

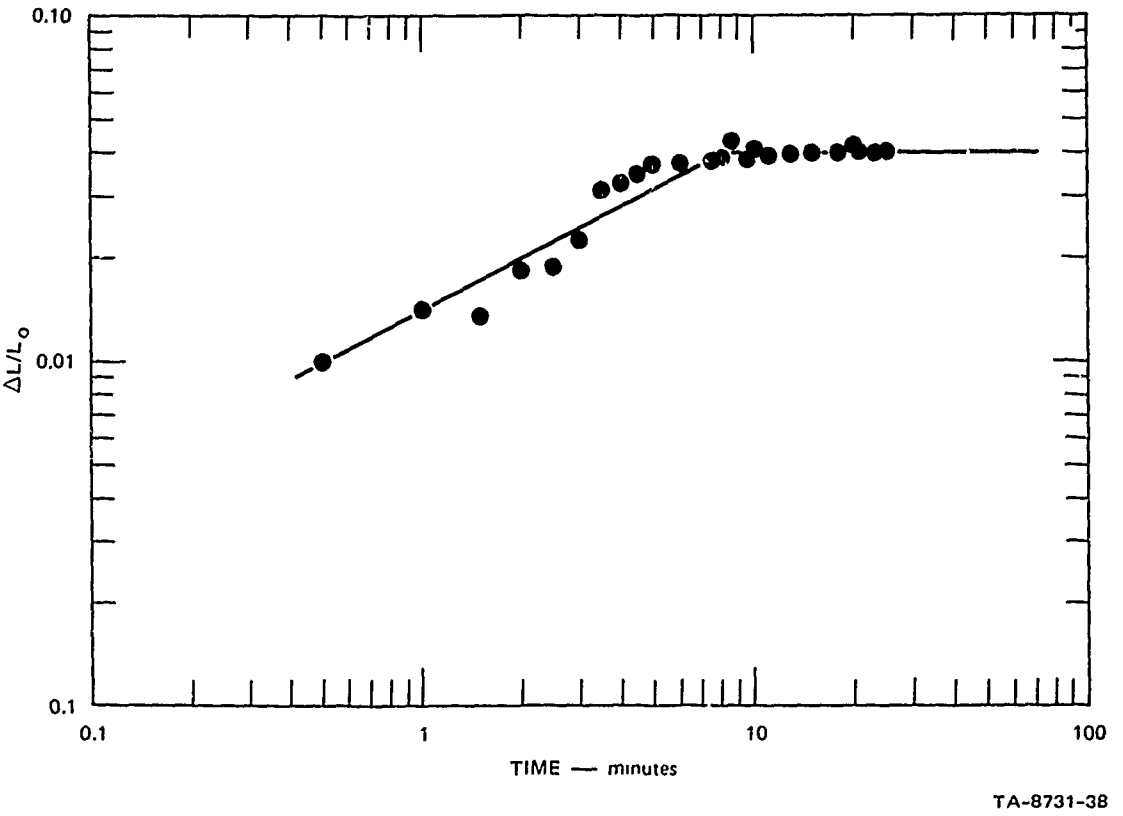

FIGURE 3 LINEAR SHRINKAGE OF $SmCo_5$ SINTERED AT 1125°C

However, the total shrinkage is greater than 4%, since this figure is only the shrinkage occurring during the solution-precipitation stage. Although the coalescence stage is shown as a plateau, solid-state sintering is occurring in the final stage and small increases in density will occur.

If the sintering temperature is below 1075°C, we note a decrease in the linear shrinkage that is greater than would be expected from the change in temperature. The Sm-Co phase diagram shows a $SmCo_2$ compound, and since reaction occurs between the 60% Sm additive and the $SmCo_2$ phase, the amount of liquid phase is decreasing and may actually disappear during these low temperature shrinkage measurements. The rate of sintering and degree of densification generally increase with the amount of liquid phase, and this could explain the decreased rates that appear to be anomalous with temperature. The amount of liquid phase can also affect grain growth kinetics in a system that sinters by a liquid phase mechanism. Further data are therefore required before a definite description can be made of the sintering of $SmCo_5$. However, at this point, the data indicate that a phase boundary reaction is rate controlling through the intermediate stages rather than a diffusion mechanism, which is not unreasonable when we consider the fact that samarium oxide is undoubtedly found on the surface of the $SmCo_5$ particles and this oxide phase must be taken into solution before considerable amounts of densification can occur.

VII OXIDATION KINETICS

Indirect evidence suggests that surface oxidation is detrimental to the magnetic coercivity of rare earth cobalt alloys.[4] At the present time, there is insufficient information on the surface oxidation of these alloys or the solubility and diffusion of oxygen within the alloys. Data are needed at melting and sintering temperatures and also at lower temperatures encountered during the grinding and storage of fine magnetic alloy particles. Some oxidation may be occurring from low levels of contaminants in glove boxes, and small amounts of surface oxide formed at modest temperatures may be sufficient to lower magnetic coercivity drastically. It is particularly important to obtain information on surface oxidation at low oxygen pressures.

A. Thermodynamic Considerations and Possible Oxidation Behavior

The rare earth oxides are extremely stable compounds, but rare earth metals and alloys are unstable with respect to oxygen at the lowest attainable operational oxygen pressures. For example, the reaction

$$2Pr(c) + \frac{3}{2} O_2(g) \overset{K_1}{\rightleftharpoons} Pr_2O_3(c) \qquad (1)$$

has an equilibrium oxygen pressure from 10^{-200} to 10^{-50} atm in the temperature range from 25°C to 800°C. The alloy reaction is similar but includes a lower chemical activity of praseodymium

$$2\underline{Pr} + \frac{3}{2} O_2(g) \overset{K_2}{\rightleftharpoons} Pr_2O_3 \qquad (2)$$

If it is assumed that the chemical activity of praseodymium in the

intermetallic compound $PrCo_5$ is proportional to its mole fraction, the equilibrium oxygen partial pressures are only doubled, which is an insignificant effect for the extremely low equilibrium oxygen pressure over the $20^{\circ}C$ to $800^{\circ}C$ temperature range.

Clearly, any oxygen in the presence of $PrCo_5$ or other rare earth magnetic alloys will be unstable and will tend to form the rare earth oxide. The extent to which an oxide film is actually formed depends on the kinetics of the surface oxidation reaction (including nucleation) or associated transport processes that bring oxygen to the surface.

Oxygen will also dissolve in these alloys to some extent, and the following equilibrium describes the solubility limit for dissolved oxygen in equilibrium with the praseodymium component of the alloy:

$$PrO_3 \overset{K_3}{\rightleftharpoons} 2\underline{Pr} + \underline{3O} \qquad (3)$$

where the maximum solubility is $a^{\circ}_{\underline{O}} = K_3^{1/3} a_{Pr}^{-2/3}$. Hence, the oxygen activity at the surface, $a^{s}_{\underline{O}}$, is equal to $a^{\circ}_{\underline{O}}$ and invariant with all experimental oxygen pressures, provided that the temperature is held constant. The oxygen activity in the interior of the alloy depends on the rate at which dissolved oxygen will diffuse into the alloy.

Both surface oxidation and internal diffusion will have temperature dependent rates and both may be occurring to a significant extent simultaneously.

B. Experimental Apparatus and Procedure

A novel apparatus has been designed to study oxidation kinetics at very low pressures over a wide temperature range. This apparatus, shown in Figure 4, is now being used to study the oxidation of $SmCo_5$. The

rate of oxygen consumption by the specimen is determined from the measured rate of decrease in oxygen pressure. To obtain adequate sensitivity and cover a large range of oxygen pressures, a zirconia electrochemical cell is being used as the oxygen sensor. This device has been used by a number of investigators to determine oxygen partial pressures or equivalent activities in gas mixtures. Recently a detailed study[9] was made of accuracy limits on a zirconia electrochemical cell measuring oxygen activities in oxygen gas and a variety of gas mixtures. Accuracies of $\pm$11% or better were reported in all instances over an oxygen partial pressure range from 10^{-18} to 1 atm. The zirconia cell used in our oxidation apparatus employs air as a reference electrode and is being operated at approximately 1000K.

The oxidation apparatus consists of an all-bakeable, ultrahigh vacuum system that includes a titanium getter ion pump and a molecular sieve sorption forepump, shown schematically in Figure 5. The specimen, generally in the form of a thin layer of closely sized coarse particles, is heated in a small cold wall vacuum furnace. The furnace consists of a small resistance heating coil mounted on a vertical axis with the specimen resting on a 1-cm dia. platinum pan located in the center of the coil. A fine wire platinum-rhodium thermocouple is welded to the bottom of the sample pan. The heating element, heat shields, and all structural support members of this furnace are constructed of platinum to eliminate extraneous oxidation. The furnace is mounted well above the supporting header to prevent the heating of thermocouple feedthroughs.

A second furnace is being used to verify results obtained with the cold wall furnace and to provide higher temperature capability. Either furnace can be removed from the vacuum system if the connecting parts are flanged shut. The secondary specimen furnace is a vacuum tight recrystallized alumina tube heated by an external resistance heating element. The specimen rests in a platinum boat within this horizontal tube furnace.

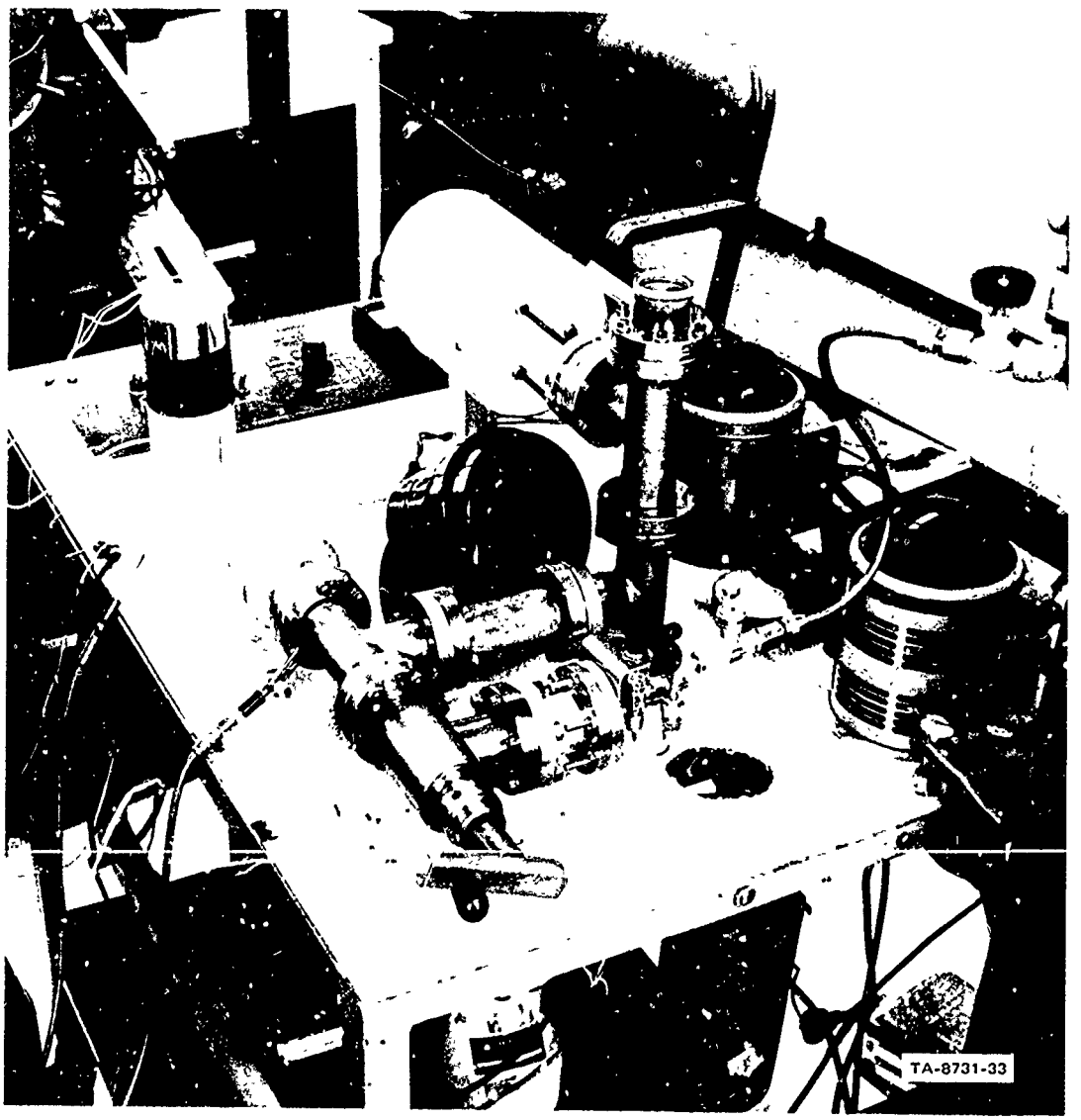

FIGURE 4 OXYGEN SORPTION APPARATUS

rate of oxygen consumption by the specimen is determined from the measured rate of decrease in oxygen pressure. To obtain adequate sensitivity and cover a large range of oxygen pressures, a zirconia electrochemical cell is being used as the oxygen sensor. This device has been used by a number of investigators to determine oxygen partial pressures or equivalent activities in gas mixtures. Recently a detailed study[9] was made of accuracy limits on a zirconia electrochemical cell measuring oxygen activities in oxygen gas and a variety of gas mixtures. Accuracies of $\pm$11% or better were reported in all instances over an oxygen partial pressure range from 10^{-18} to 1 atm. The zirconia cell used in our oxidation apparatus employs air as a reference electrode and is being operated at approximately 1000K.

The oxidation apparatus consists of an all-bakeable, ultrahigh vacuum system that includes a titanium getter ion pump and a molecular sieve sorption forepump, shown schematically in Figure 5. The specimen, generally in the form of a thin layer of closely sized coarse particles, is heated in a small cold wall vacuum furnace. The furnace consists of a small resistance heating coil mounted on a vertical axis with the specimen resting on a 1-cm dia. platinum pan located in the center of the coil. A fine wire platinum-rhodium thermocouple is welded to the bottom of the sample pan. The heating element, heat shields, and all structural support members of this furnace are constructed of platinum to eliminate extraneous oxidation. The furnace is mounted well above the supporting header to prevent the heating of thermocouple feedthroughs.

A second furnace is being used to verify results obtained with the cold wall furnace and to provide higher temperature capability. Either furnace can be removed from the vacuum system if the connecting parts are flanged shut. The secondary specimen furnace is a vacuum tight recrystallized alumina tube heated by an external resistance heating element. The specimen rests in a platinum boat within this horizontal tube furnace.

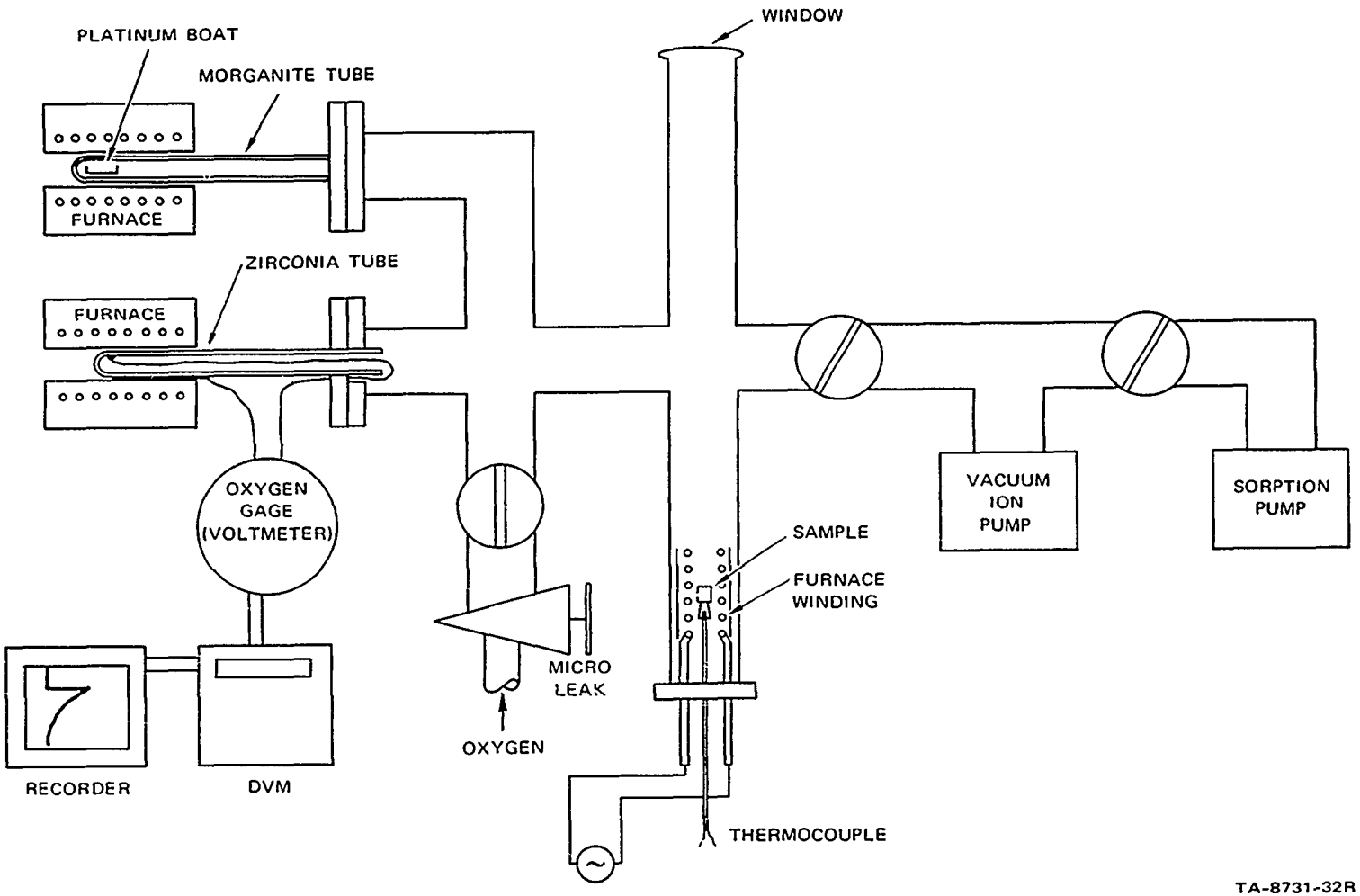

FIGURE 5 SCHEMATIC DRAWING OF OXYGEN SORPTION APPARATUS

Although this furnace has more heated surfaces for outgassing or gettering oxygen, it does provide a more uniform thermal environment and better temperature control.

Before an experiment can be begun, the system must be leak-free, outgassed, and free of oxygen gettering contaminants. These conditions are verified by suitable tests that are conducted before each sample experiment. Each sample is usually subjected to a series of isothermal runs without being removed from the apparatus. Before each run the system is evacuated, and the ion pump is valved shut so that a closed system of known constant volume contains the specimen. Each run is an isothermal batch experiment performed by introducing an aliquot of oxygen through a microleak valve at the beginning of the run. The instantaneous rise and subsequent decrease in oxygen pressure produces a corresponding voltage output from the zirconia cell that is followed with a digital voltmeter and stripchart recorder.

The zirconia cell temperature is controlled automatically. The specimen temperature is controlled either automatically or manually and recorded.

The zirconia cell E.M.F. digital data, V_o, at different elapsed times are collected and read into a computer program that calculates and graphs oxygen pressure versus time

$$p_{O_2} = p_{O_{2_{ref}}} \exp^{-4FV/RT_{cell}} \qquad (4)$$

where the reference pressure, $p_{O_{2_{ref}}}$ is 0.21 atm; F is 23,061 cal per volt equivalent; T_{cell} is the absolute zirconia cell temperature; and R is the gas constant. Input data also include the cell temperature; specimen

temperature, T_s; volume of the system, V_o; and total surface area of the specimen, A_s.

The oxygen aliquot, Q_{O_2}, is calculated from the initial pressure and system volume. The primary oxygen pressure versus time data are used to compute and graph secondary data and coefficients for testing various hypothesized rate mechanisms. The secondary output data are:

1. Moles oxygen sorbed, Q_i, versus time, t_i

$$Q_i = Q_{i-1} + \frac{V_o}{RT_g}\left(p_{O_2}{}_{i-1} - p_{O_2}{}_{i}\right) \tag{5}$$

where the average gas temperature in the vacuum system, T_g, was estimated to be 305K.

2. Moles oxygen sorbed per unit area, q_i, versus time, t_i

$$q_i = Q_i/A_s \quad . \tag{6}$$

3. Oxygen flux, J_i, versus time, t_i

$$J_i = \frac{V_o}{2RT_g A_s}\left(p_{O_2}{}_{i-1} - p_{O_2}{}_{i-1}\right) . \tag{7}$$

4. First order rate constant, k_{O_2}, versus time, t_i

$$k_{O_2(i)} = J_i/p_{O_2}{}_{i} \quad . \tag{8}$$

5. Monatomic oxygen (one-half order) rate constant, $k_{\underline{O}}$, versus time, t_i

$$k_{\underline{O}(i)} = J_i/p_{O_2}{}_{i}^{\frac{1}{2}} \quad . \tag{9}$$

This rate law assumes that surface adsorption and splitting of the O_2 molecule occurs before chemical reaction.

6. Parabolic rate constant, k_p, versus time, t_i

$$k_{p_{(i)}} = q_i t_i^{-\frac{1}{2}} . \tag{10}$$

This coefficient assumes that quasi-steady state diffusion through a protective oxide film covering the surface controls the rate of oxide growth. It would also describe the initial stages of diffusion into the alloy from a fixed surface oxygen concentration, $a_{\underline{O}}^{s} = a_{\underline{O}}^{\circ}$, since

$$q_i = a_{\underline{O}}^{s} \left(\frac{D_O t_i}{\pi} \right)^{\frac{1}{2}} \tag{11}$$

provided that all of the surface oxide is dissolved so that q_i represents only oxyger absorbed by the internal diffusion process.

7. Fractional oxygen uptake versus time, t_i, and square root of time, $t_i^{\frac{1}{2}}$, were graphed

$$F_{(i)} = \frac{Q_i}{Q_\Omega} . \tag{12}$$

8. The log parabolic rate constant versus log oxygen pressure was graphed.

C. Results

Some interesting initial oxidation results have been obtained with $SmCo_5$. However, insufficient experiment data have been accumulated on which to base final conclusions. All of the experiments to date have been

run on an arc melted $SmCo_5$ alloy hand ground to -100 mesh. The oxygen content of this alloy, including surface oxide, was determined before any surface oxidation tests were performed, but after the alloy had been stored in air for several weeks following grinding. Neutron activation analysis showed that the starting oxygen content was 0.198% $\pm$ 0.016%.

Experiments will continue with the above arc melted alloy, a commercial alloy, and an alloy produced by metallothermic reduction. To date, runs have been made only at temperatures of 105°C or higher, but the oxidation rate is appreciable at the lowest temperature investigated.

Some of the results from a typical run at 200°C are shown in Figure 6. Note that the oxygen flux decreases with time so it can be concluded that the rate depends on the oxygen pressure, i.e., it is not a zero order chemical kinetic process. The one-half order rate constant decreases with time suggesting that a one-half order rate mechanism is not followed. The parabolic rate constant shows considerable variation with time, suggesting that the parabolic rate mechanisms are inappropriate.

The first order rate constant shows little variation out to at least 95% of the gas reacted. The variation is usually less than $\pm$35%, which is fairly good uniformity for an experimental rate constant. These data are fairly typical of the runs at 200°C and higher temperatures and suggest that the oxidation kinetics are described by a simple irreversible first order rate process

$$\frac{dN_{O_2}}{A_s dt} = -k_{O_2} p_{O_2} .$$

The rate constant increases with temperature and appears to behave in the usual manner for an activated process

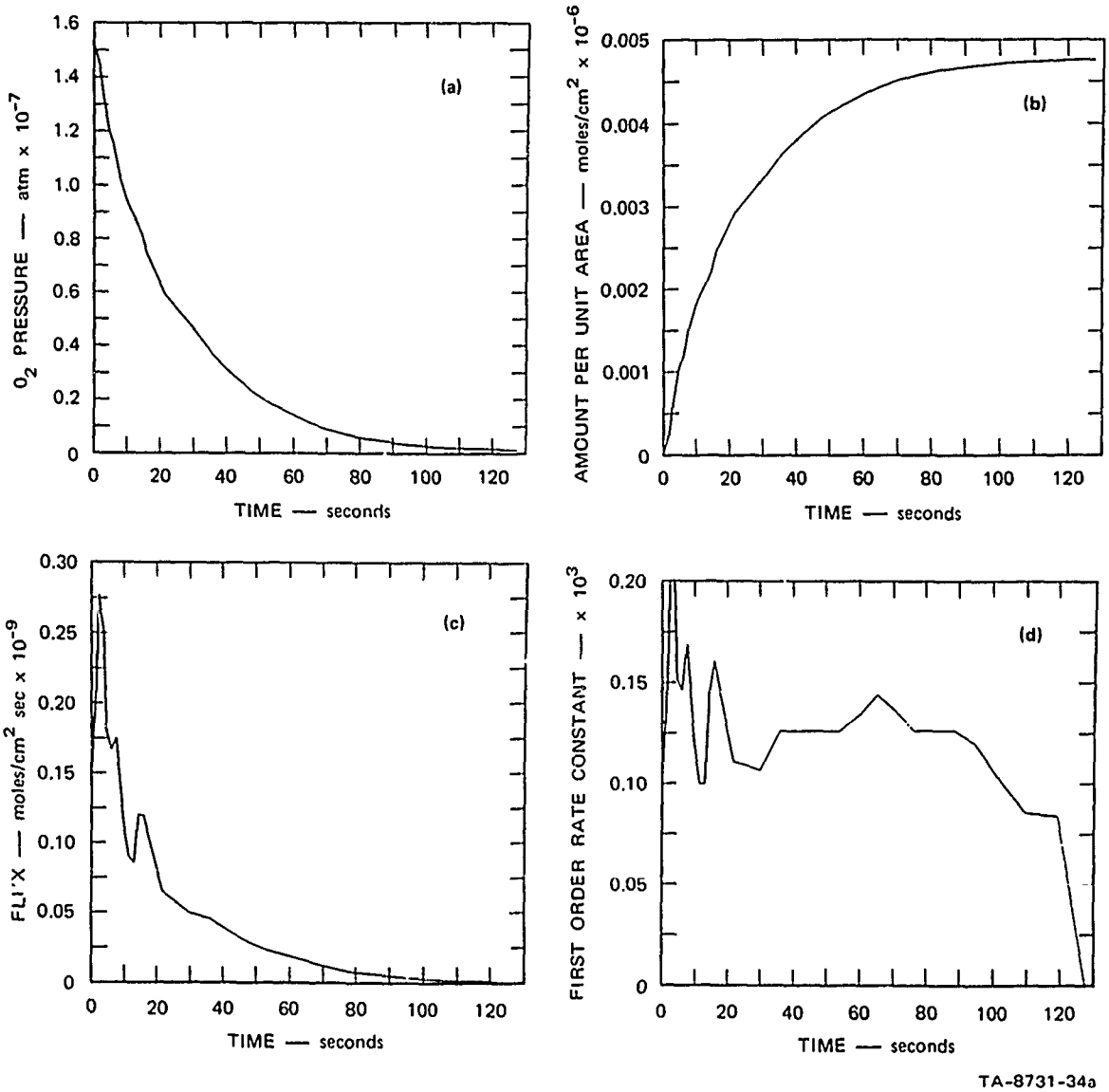

FIGURE 6 OXIDATION EXPERIMENT ON $SmCo_5$ SAMPLE 8, RUN 8, 200°C

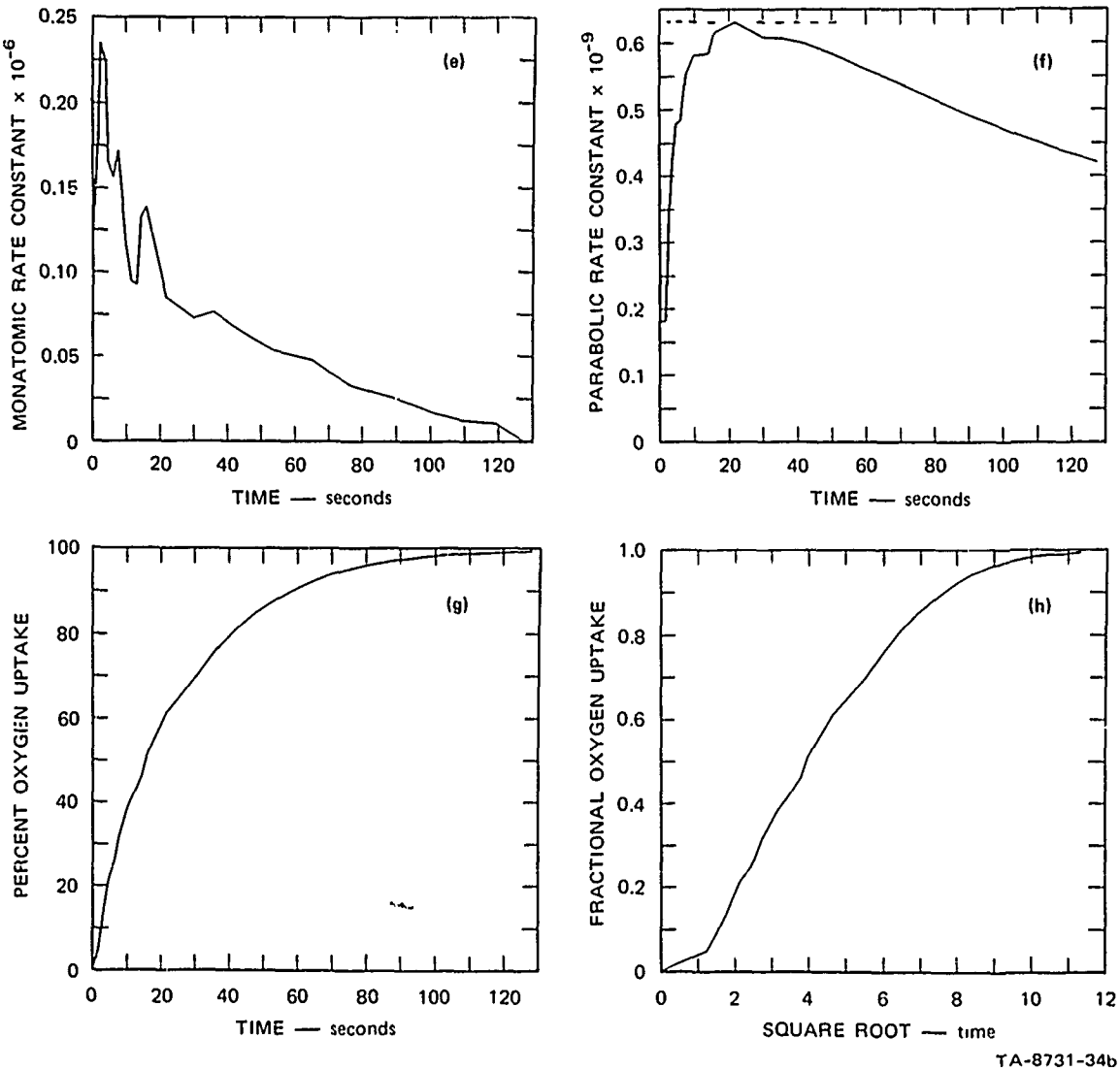

FIGURE 6 OXIDATION EXPERIMENT ON $SmCo_5$ SAMPLE 8, RUN 8, 200°C (Concluded)

$$k_{O_2} = k' \exp^{-\Delta H^{\ddagger}/RT} \exp^{\Delta S^{\ddagger}/R} .$$

The activation enthalpy, $\Delta H^{\ddagger}$, is less than 15 Kcal g-mole^{-1} but insufficient data are available to report this more accurately.

A Hertz-Langmuir calculation of the rate was made to determine an effective rate constant limited only by gas collision theory .

$$k_{H-L} = (2\pi M_{O_2} RT)^{-\frac{1}{2}} .$$

The result was $\sim 10^{9}$ greater than the experimentally observed values of k_{O_2}. Although the target area exposed for molecular collision may be only 1% to 10% of the total particle area, this is insufficient to account for the large difference in calculated and experimental rate constants. Therefore, the rate does not appear to be limited by oxygen transport in the gas phase at the moderately low oxygen pressures used in the oxidation experiments.

The maximum value of the parabolic rate constant was plotted versus the initial oxygen aliquot, Q_{Ω}, over several decades of both parameters and at various temperatures, (see Figure 7). The maximum values of the parabolic rate constant do not correlate with temperature as would be expected if this mechanism were rate controlling. They are directly proportional to the oxygen aliquot, which should not occur if the parabolic mechanism is rate controlling. Run specimen temperatures (^{o}C) are superimposed on the data points in Figure 7 and these results further confirm that diffusion processes are not rate-controlling above 200^{o}C.

Although we have few data below 200^{o}C, it appears that there may be a change in mechanism entailing an initial fast oxidation step followed by partial oxide film passivation and slower subsequent oxidation. This

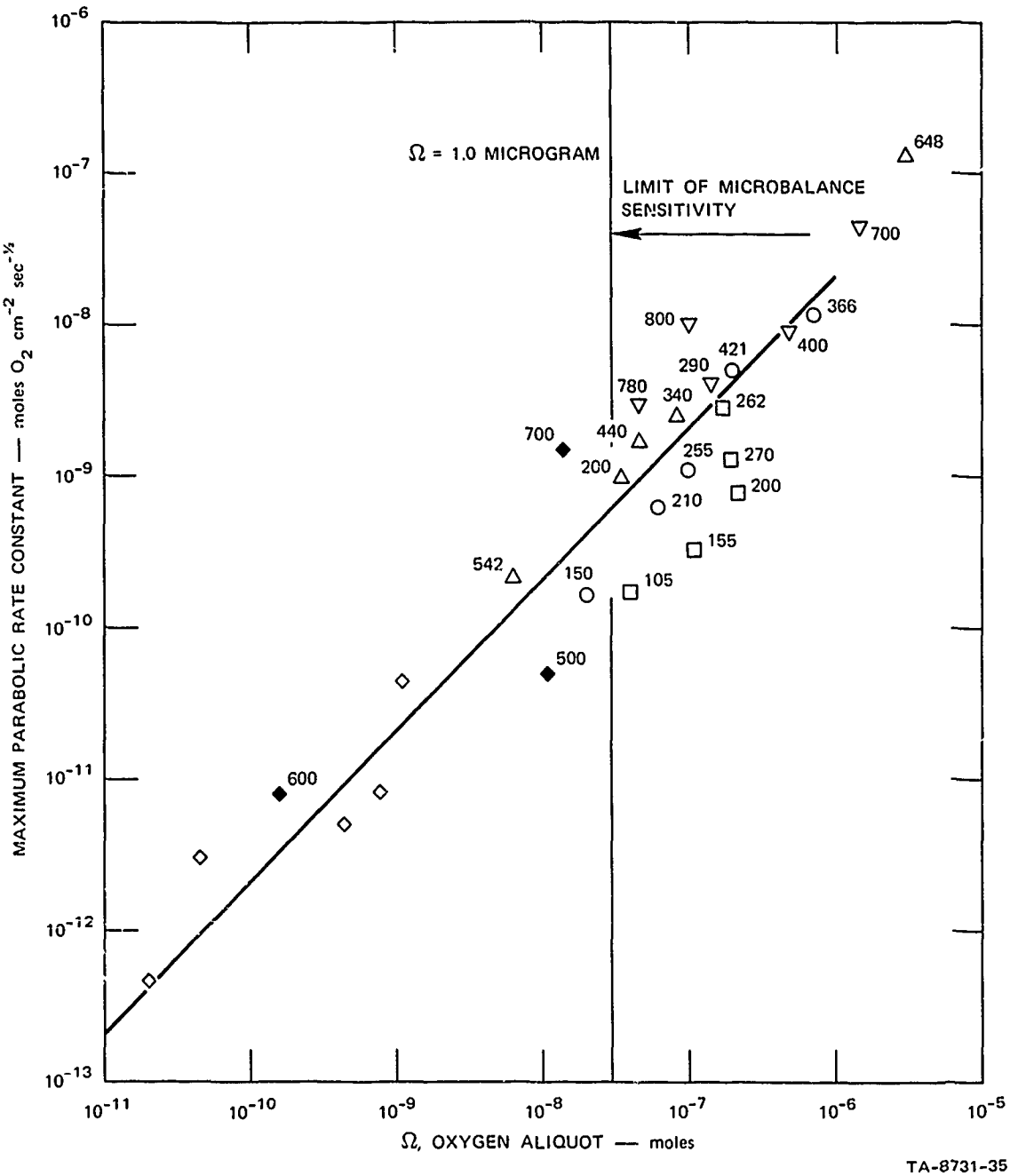

FIGURE 7 VARIATION IN THE MAXIMUM CALCULATED PARABOLIC RATE CONSTANT WITH THE OXYGEN ALIQUOT

phenomenon has been observed in some runs above 200°C but is more clearly illustrated at low temperatures (see Figure 8). The decrease in the first order rate constant approaches an order of magnitude but it subsequently increases.

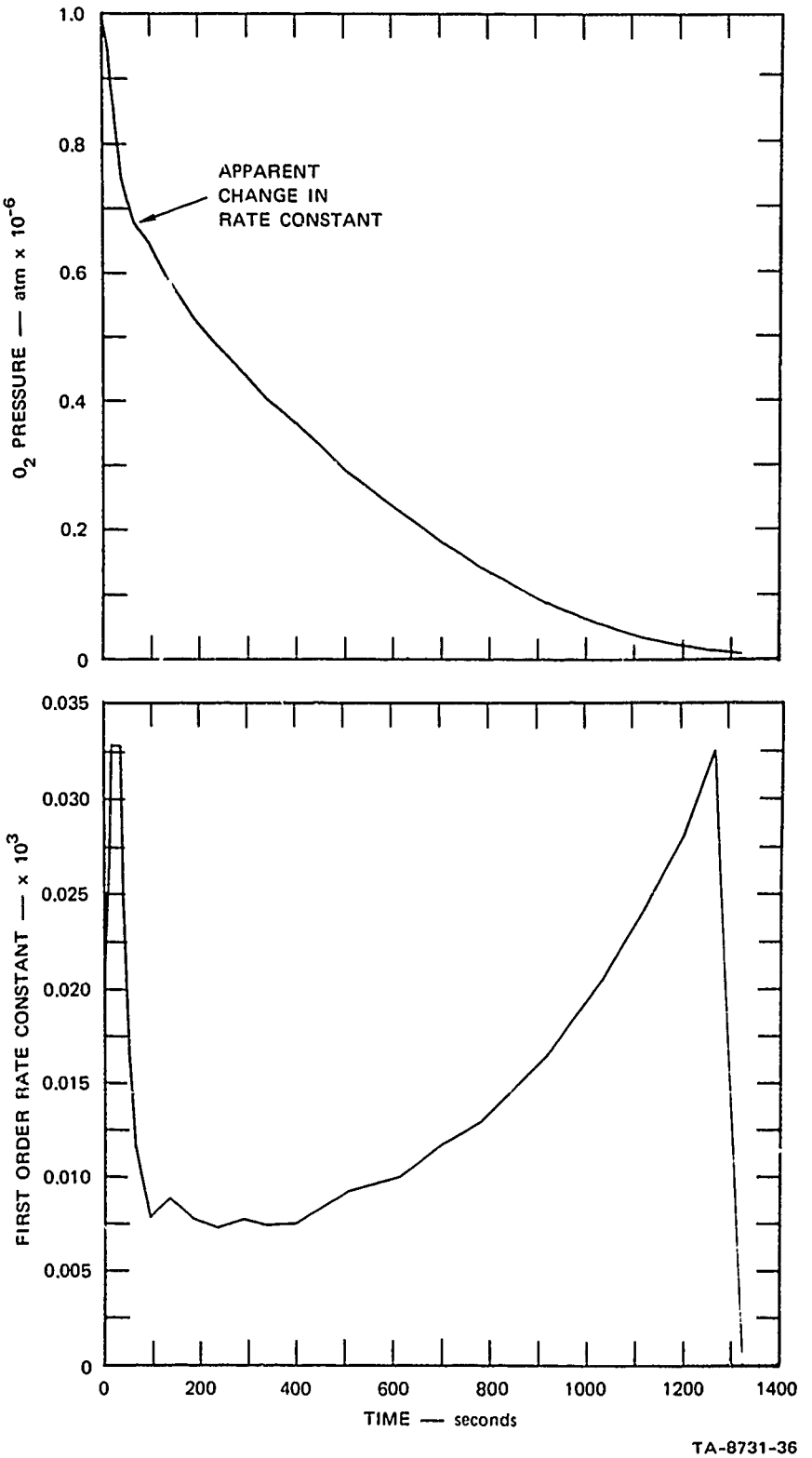

FIGURE 8 OXIDATION OF $SmCo_5$ AT 105°C SHOWING REDUCTION IN RATE CONSTANT WITH TIME

FUTURE WORK

The work planned for the following period will emphasize a continuation of present studies: (1) sintering kinetic studies, (2) magnetic evaluation of powders and sintered magnets, (3) oxidation kinetics of $SmCo_5$ and $PrCo_5$, and (4) metallothermic reduction of $SmCo_5$ and other $RECo_5$ alloys.

REFERENCES

1. J. J. Becker, J. Appl. Phys. 39, 1270-71 (1968)
2. K. Strnat et al., J. Appl. Phys. 38, 1001 (1967)
3. J. J. Becker, IEEE Trans. Magnetics, MAG-4, 239-249 (1968)
4. P. J. Jorgensen and R. W. Bartlett, "Materials Processing of Rare Earth-Cobalt Permanent Magnets," Technical Report AFML-TR-71-188, August 1971
5. G. H. S. Price, C. J. Smithells and S. V. Williams, J. Institute of Metals 62, 239 (1938)
6. F. V. Lenel, Trans. AIME 175, 878 (1948)
7. W. D. Kingery, J. Appl. Phys. 30, 301 (1959)
8. A. L. Prill, H. W. Hayden, and J. H. Brophy, Trans. AIME 233, 960 (1965)
9. T. H. Etsell and S. N. Flengas, Metallurgical Trans. 3, 27-36 (1972).